

# Predicting calvarial growth in normal and craniosynostotic mice using a computational approach

Arsalan Marghoub,<sup>1</sup> Joseph Libby,<sup>2</sup> Christian Babbs,<sup>3</sup> Erwin Pauws,<sup>4</sup> Michael J. Fagan<sup>2</sup> and Mehran Moazen<sup>1</sup> 

<sup>1</sup>Department of Mechanical Engineering, University College London, London, UK

<sup>2</sup>Medical and Biological Engineering, School of Engineering and Computer Science, University of Hull, Hull, UK

<sup>3</sup>MRC Molecular Haematology Unit, MRC Weatherall Institute of Molecular Medicine, University of Oxford, Oxford, UK

<sup>4</sup>Institute of Child Health, Great Ormond Street, University College London, London, UK

## Abstract

During postnatal calvarial growth the brain grows gradually and the overlying bones and sutures accommodate that growth until the later juvenile stages. The whole process is coordinated through a complex series of biological, chemical and perhaps mechanical signals between various elements of the craniofacial system. The aim of this study was to investigate to what extent a computational model can accurately predict the calvarial growth in wild-type (WT) and mutant type (MT) *Fgfr2*<sup>C342Y/+</sup> mice displaying bicoronal suture fusion. A series of morphological studies were carried out to quantify the calvarial growth at P3, P10 and P20 in both mouse types. MicroCT images of a P3 specimen were used to develop a finite element model of skull growth to predict the calvarial shape of WT and MT mice at P10. Sensitivity tests were performed and the results compared with *ex vivo* P10 data. Although the models were sensitive to the choice of input parameters, they predicted the overall skull growth in the WT and MT mice. The models also captured the difference between the *ex vivo* WT and MT mice. This modelling approach has the potential to be translated to human skull growth and to enhance our understanding of the different reconstruction methods used to manage clinically the different forms of craniosynostosis, and in the long term possibly reduce the number of re-operations in children displaying this condition and thereby enhance their quality of life.

**Key words:** biomechanics; development; calvarial bones; sutures; finite element method; craniosynostosis.

## Introduction

The mammalian cranial vault principally consists of five flat bones joined along their edges by soft tissues termed sutures (Opperman, 2000; Morriss-Kay & Wilkie, 2005; Herring, 2008). The sutures are the sites where most skull vault growth occurs and they also function to give bones flexibility for birth and to allow the skull to expand and grow as the brain enlarges (Cohen, 2005; Richtsmeier & Flaherty, 2013). Premature closure of the sutures, or craniosynostosis, is a medical condition that occurs in about 1 in 2500 births; the question of an increase in the occurrence rate has been raised (Boulet et al. 2008; van der Meulen et al. 2009; Johnson & Wilkie, 2011; Cornelissen et al. 2016). The majority of

cases (70%) are non-syndromic, i.e. single suture synostosis, with the remaining instances being syndromic (e.g. Crouzon and Apert), in which more than one suture fuses and where additional features are present such as midfacial hypoplasia (Morriss-Kay & Wilkie, 2005). Children displaying craniosynostosis generally require a surgical procedure that in the majority of cases is carried out at 6–12 months of age.

Research to understand the genetic basis and clinical course of craniosynostosis (Wilkie, 1997; Morriss-Kay & Wilkie, 2005; Al-Rekabi et al. 2016) has led to the development of various animal models (Mooney et al. 1998; Grova et al. 2012; Holmes, 2012). Mice have been investigated extensively in this area because murine calvarial morphology and genetics share several similarities with humans, with the advantage that the developmental process occurs over a much shorter period (Morriss-Kay & Wilkie, 2005). In terms of calvarial development the intracranial volume (ICV) of wild-type (WT) mice typically reaches 70% of the adult size by postnatal day 10 (P10) with minimal further growth after P20 (Aggarwal et al. 2009; Moazen et al. 2016). In contrast, human ICV reaches 65% of the adult

### Correspondence

Mehran Moazen, Department of Mechanical Engineering, University College London, Torrington Place, London WC1E 7JE, UK.

T: +44 (0)207 679 3862; E: m.moazen@ucl.ac.uk

Accepted for publication 21 November 2017

Article published online 15 December 2017

volume by 1 year, with minimal further growth after 10 years (Dekaban, 1977; Sperber, 1989).

The Crouzon mouse model (*Fgfr2*<sup>C342Y/+</sup>) has been extensively studied and has become well-established for investigating craniosynostosis (Eswarakumar et al. 2004; Perlyn et al. 2006; Liu et al. 2013; Martínez-Abadías et al. 2013; Peskett et al. 2017). This line is particularly interesting, as it exhibits robust phenotypic abnormalities with features recapitulating clinical abnormalities observed in patients. The coronal sutures (joining the parietal and frontal bones) are primarily affected in these mice, as well as other joints on the cranial base (e.g. intersphenoidal synchondrosis joining the presphenoid and basisphenoid bones), causing a predictable brachycephalic (wide and short) head shape also characteristic of Crouzon patients (Eswarakumar et al. 2004; Perlyn et al. 2006; Liu et al. 2013). Coronal sutures in the WT mouse are immediately adjacent but never fully ossified, i.e. with a micrometer gap being present between the adjacent bones. In the Crouzon mouse, overlapping of the frontal and parietal bones at this suture begins at the embryonic stages (E18.5), with full ossification (closure) occurring at ~P20 (Eswarakumar et al. 2004; Perlyn et al. 2006; Peskett et al. 2017). Thus, Crouzon *Fgfr2*<sup>C342Y/+</sup> mutant type (MT) and WT mice provide an invaluable tool with which to understand the biomechanics of craniosynostotic and normal skull growth during postnatal development.

The finite element (FE) method is a computational modelling technique that has been widely used to understand general craniofacial biomechanics (e.g. Ross et al. 2005; Rayfield, 2007; Curtis et al. 2011; Cox et al. 2012; Moazen et al. 2013; Gussekloo et al. 2017), but it also has great potential in the simulation of growth and development of the craniofacial system. It can be used to predict the calvarial growth and to optimize reconstruction of various forms of craniosynostosis (Li et al. 2013; Wolanski et al. 2013; Libby et al. 2017). However, FE models require several input parameters and the results produced must be validated using experimental data generated *in vitro* or *in vivo* (e.g. Kupczik et al. 2007; Szwedowski et al. 2011; Toro-Iba-cache et al. 2016). To the best of our knowledge, there have not been any detailed simulations of skull growth (normal or craniosynostotic) which could lead to improvements in patient management or improvement of craniofacial surgery.

This study tests the hypothesis that brain expansion during postnatal development drives calvarial growth and the response of the calvarial bone and sutures govern the resulting skull shape. We tested this hypothesis in an FE study to simulate calvarial growth. Specific aims were: (i) to quantify the postnatal calvarial growth in WT and MT mice at P3, 10 and 20; (ii) to develop a FE model of mouse calvarial growth; and (iii) to validate the FE predictions by comparing them with *ex vivo* measurements of the calvaria in WT and MT mouse models.

## Materials and methods

Micro-computed tomography (microCT) images were obtained from WT and mutant, *Fgfr2*<sup>C342Y/+</sup>, mice. A series of morphological studies were carried out to quantify the calvarial growth at P3, P10 and P20. The microCT data of a single P3 mouse were then used to develop an FE model to simulate skull growth and in particular to predict mean calvarial shape at P10. P10 was chosen as 70% of skull growth has been completed at this stage, with the P20 data included to confirm this (see also Chuang et al. 2011; Moazen et al. 2016). Several modelling sensitivity tests were performed and the results compared with a mean specimen identified from the morphological study. This FE model was then used in the same way but with specified premature fusion of the presphenoid-basisphenoid synchondrosis (PBS), frontal, coronal, and lambdoid sutures to simulate growth to the equivalent P10 (MT) mutant geometry.

## Morphological analysis

MicroCT scans of 22 WT and MT mice at P3 ( $n = 1$  for WT and MT), P10 ( $n = 5$  for WT and MT), and P20 ( $n = 5$  for WT and MT) were

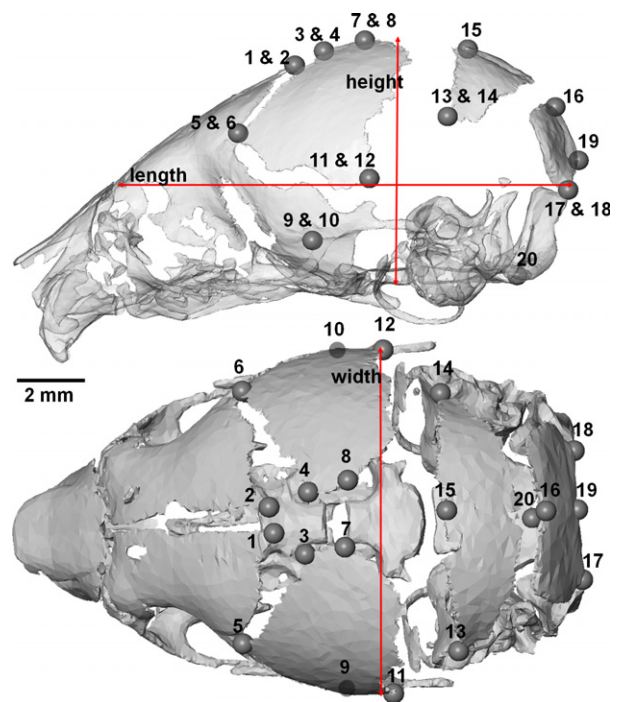


**Fig. 1** Lateral and dorsal view of a P3 mouse skull, highlighting landmark positions, length, height and width measurement. 1 & 2: Most medial intersection of the frontal and parietal bones, on the frontal (left & right); 3 & 4: Most medial intersection of the frontal and parietal bones, on the parietal (left and right); 5 & 6: Most lateral intersection of the frontal and parietal bones, on the frontal (left and right); 7 & 8: Midpoint on medial side of the parietal bone (left & right); 9 & 10: The posterior root of the zygomatic process (left & right); 11 & 12: Most posterior-inferior point on the parietal (left and right); 13 & 14: Most posterior-inferior point on the interparietal (left & right); 15: Most anterior-medial point of the interparietal bone; 16: Most anterior-medial point of the occipital bone; 17 & 18: Most posterior-lateral point of the occipital bone; 19: Most posterior-medial point of the occipital bone; 20: Most posterior-medial point of the basioccipital bone.

obtained using an X-Tek HMX160 microCT scanner (XTek Systems Ltd, Tring, UK). The images had a voxel size of 0.02 mm in all directions. Avizo image processing software (FEI Visualization Sciences Group, Merignac Cedex, France) was used to reconstruct these data into three-dimensional models. The models were positioned so that in the mid-sagittal and transverse planes the basisphenoid and presphenoid bones were aligned with the horizontal axis. Following this alignment, calvarial length was measured in the mid-sagittal plane as the distance between the most anterior part of the frontal suture and the most posterior part of the calvaria (Fig. 1). Calvarial height was measured in the mid-sagittal plane as the distance between the basisphenoid and the most superior part of the calvaria. Finally, calvarial width was measured in the transverse plane as the distance between the two most lateral points of the calvaria. An average specimen at each age and in each group was identified based on the specimen with the closest length, width and height to the mean values.

## Finite element analysis

### Model development

A three-dimensional model of the P3 WT mouse was developed from the microCT data (Fig. 2), with bone and sutures segmented and reconstructed in Avizo. The ICV was defined by filling the whole ICV, hence it was necessary to ensure that the skull was fully enclosed. Thus the foramen magnum was filled, and areas of the calvaria that were not fully developed were also defined manually. The model eventually consisted of 23 different sections. A surface model of the skull was then transformed into a meshed solid geometry using Avizo and was then imported into an FE software ANSYS v.14.5 (ANSYS Inc., Canonsburg, PA, USA). The model was meshed

using SOLID187 tetrahedral elements (10 node elements with quadratic displacement behaviours), which are well suited for modelling irregular geometries (ANSYS Theoretical Manual, v. 14.5). Mesh convergence was carried out, with the final model defined by over 144 000 elements.

### Material properties

All regions were assigned isotropic material properties. In the baseline model, an elastic modulus of 3500 MPa was assumed for the bone. This was based on extrapolation of the frontal and parietal bone properties measured in mice at P10, P20 and P70 (Moazen et al. 2015). Sutures and undeveloped areas of bone were assigned an elastic modulus of 30 MPa (Henderson et al. 2005; Moazen et al. 2015) and brain (the ICV) was modelled with an elastic modulus of 150 MPa. A Poisson's ratio of 0.3 was used for all the materials, except 0.48 for the brain (Claessens et al. 1997).

### Boundary conditions and loading

The ICV expansion during calvarial enlargement was modelled by expansion of the ICV (Fig. 2) by applying a thermal expansion to the ICV in the FE model to increase its volume. Isotropic linear expansion was assumed using the following equation:

$$\Delta V = V1 \times \alpha \times \Delta T \quad (1)$$

where  $\alpha$  is the expansion coefficient,  $\Delta V$  the change in volume, equal to the target volume of the next age  $V2$  minus the current volume  $V1$ . The change in temperature  $\Delta T$  was set at an arbitrary constant value of 100 °C,

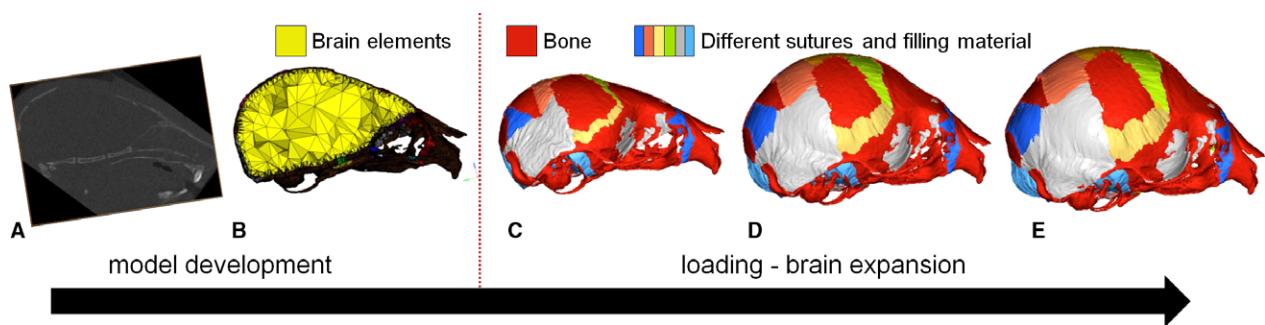


**Fig. 2** Finite element (FE) model development and loading. Micro-CT images (A) were used to develop the 3D FE model (B). Brain volume at P3 (C and yellow elements shown in B) was expanded to P10 and P20 (D and E). Note colours in (C) and (D) highlight different sections segmented, i.e. bone and sutures.

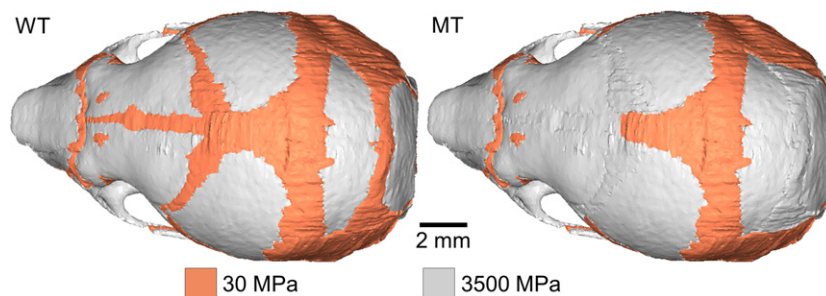


**Fig. 3** 3D elastic modulus distribution of wild-type (WT) and mutant type (MT) for finite element models. Presphenoid-basisphenoid synchondrosis, frontal, coronal, and lambdoid sutures are fused prematurely by changing their elastic modulus from suture material to that of bone (3500 MPa).

and then  $\alpha$  was altered to achieve the desired ICV volume. A thermal expansion that finally led to less than a 5% difference between the predicted brain and actual brain volume was considered acceptable. Thus, the P3 calvarium was initially expanded to the ICV of the WT P10 (Chuang et al. 2011). All degrees of freedom were constrained at three nodes on the presphenoid bone. The presphenoid bone was constrained, as quantification of the WT mouse skull growth revealed that this bone grows centrally during development and can be considered effectively to remain at the same position in the skull.

### Measurements

Twenty landmarks (LMs) were used to quantify any differences between the predicted P10 skull (from the FE model) and the *ex vivo* P10 (based on a 3D reconstruction from the CT data). Although more LMs might have increased the sensitivity of the measurements, it was challenging to reliably identify more positions in the P3 geometry due to large areas of soft tissue. See Fig. 1 for the LM details.

Root mean-square (RMS) differences between the position of the actual and predicted LMs were then calculated using the following equation:

$$\text{RMS} = \sqrt{\frac{\sum_{i=1}^n d_i^2}{n}} \quad (2)$$

where  $n$  is the number of landmarks and  $d_i$  is the distance between two corresponding landmarks of *ex vivo* P10 (in Avizo) and simulated P10 (expanded P3 geometry in ANSYS), with  $d_i$  obtained by:

$$d = \sqrt{(x_2 - x_1)^2 + (y_2 - y_1)^2 + (z_2 - z_1)^2} \quad (3)$$

It should be highlighted again that this study is focused on calvarial growth and not facial growth, therefore no LMs were assigned to the facial bones and an RMS of zero would have meant an identical match between the predicted shape and *ex vivo* results.

To quantify the change in the overall shape and to visualize the differences between the skulls, 3D distance plots were also created using Avizo. The models were aligned and the points on the expanded FE surface mesh were measured to the closest point on the average *ex vivo* skull at P10. The areas at which the two surfaces differed (both positively or negatively) showed where the FE models had over- or under-predicted skull growth. The maximum differences in both the positive and negative directions were calculated and plotted on a colour contour plot.

### Sensitivity tests

Three sensitivity tests were carried out on the WT model to investigate the sensitivity of the results to some of the key input parameters, in particular: (i) boundary condition: the baseline model in this study was constrained at the presphenoid bone; this was altered to basisphenoid or both presphenoid and basisphenoid; (ii) brain properties: there is a large range of data reported in the literature for brain properties (e.g. Miller et al. 2000; Gefen & Margulies, 2004; Bouchonville et al. 2016), therefore the baseline value of 150 MPa was altered within the range from 1 to 1500 MPa; (iii) suture properties: our previous experimental measurements (Moazen et al. 2015) showed a large standard deviation for the suture properties, therefore the baseline value of 30 MPa was varied between 3 and 300 MPa.

### Predicting mutant *Fgfr2*<sup>C342Y/+</sup> mouse calvarial shape at P10

The baseline WT model was used to predict the mutant skull shape at P10 after fusion of some of the sutures (Fig. 3). Liu et al. (2013) showed that in this mouse model, several sutures including the PBS, frontal, coronal and lambdoid sutures fuse prematurely. Therefore, they were effectively fused in the WT model described above by changing their elastic modulus from suture material to that of bone (3500 MPa). The ICV was expanded the same as the WT models and the results were compared with the microCT data of the MT mice at P10. Figure 3 shows the 3D elastic modulus distribution across the WT and MT FE models.

## Results

### Morphological analysis

Figure 4 summarizes the calvarial length, width and height measurements at P3, P10 and P20 for the WT and MT

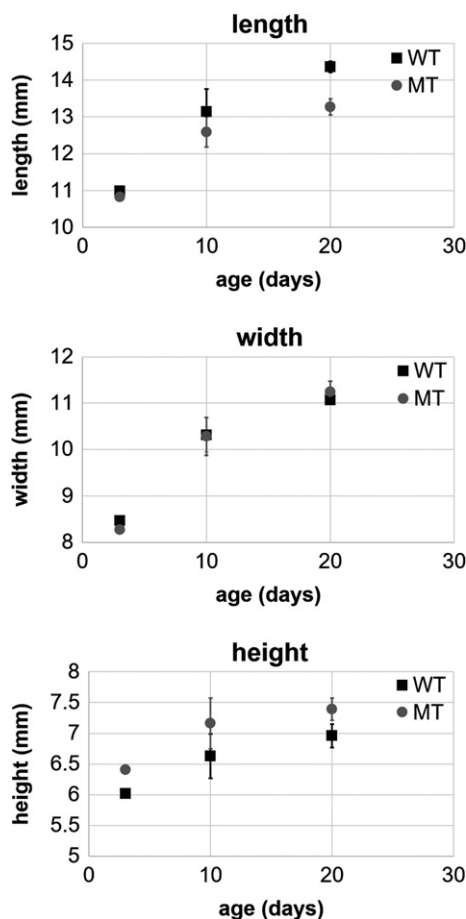


Fig. 4 Length, width and height measurement at P3 ( $n = 1$ ), P10 ( $n = 5$ ) and P20 ( $n = 5$ ). Error bars indicate the SD of each group.

models. Although all measurements increased gradually from P3 to P20, calvarial length and height of the WT mice were consistently higher and lower than the MT mice, respectively. This pattern is also evident in the 2D sagittal cross-sections of the WT and MT mice (Fig. 5).

Figure 6 compares the overall morphological differences between the *ex vivo* WT and MT mice at P10 using 3D distance colour plots. In the dorsal view, the highlighted square shows the overgrowth of the MT skull across the parietal region (bulging). In the posterior view, the highlighted oval shows the undergrowth of the lambdoid region in the MT mouse (Fig. 6).

**Finite element analysis**

*Sensitivity tests*

Altering the boundary conditions from the baseline model, i.e. at the presphenoid bone (set 2 in Fig. 7A), to the basisphenoid (set 1 in Fig. 7) or both the presphenoid and

basisphenoid (set 3, Fig. 7A) leads to overestimation of the calvarial height. At the same time, the RMS difference values were decreased from the baseline value of 1.14–1.01 and 0.96, for set 1 and 3, respectively. Altering the elastic modulus of the brain had the greatest impact on the overall skull shape (Fig. 7B). Reducing the elastic modulus of the brain led to an increase in the skull height and bulging of the fronto-parietal region. However, increasing the elastic modulus of the brain from 15 to 150 MPa and 1500 MPa led to a closer match with the overall skull shape of the *ex vivo* data and reduced the RMS values from 1.28 to 0.95 for an elastic modulus change of 15–1500 MPa. Increasing the elastic modulus of the sutures from 3 to 300 MPa led to a gradual increase in skull height and decrease of RMS values from 1.18 to 0.99 (Fig. 7C).

*Predicted WT and MT calvarial shape at P10*

Figure 8 compares the overall geometric differences (in 2D and 3D) between the FE prediction of skull shape at P10 vs.

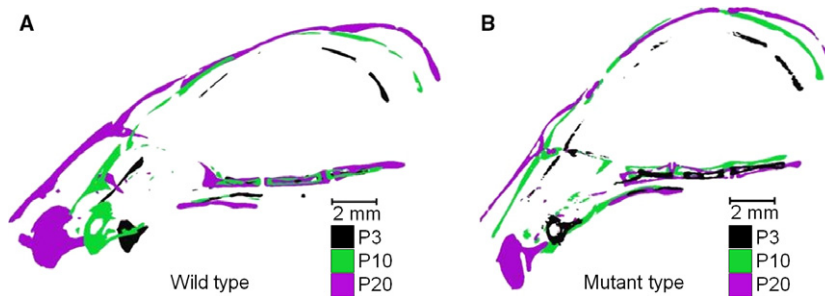


Fig. 5 Sagittal sections of *ex vivo* wild-type and mutant type mice at P3, P10 and P20.

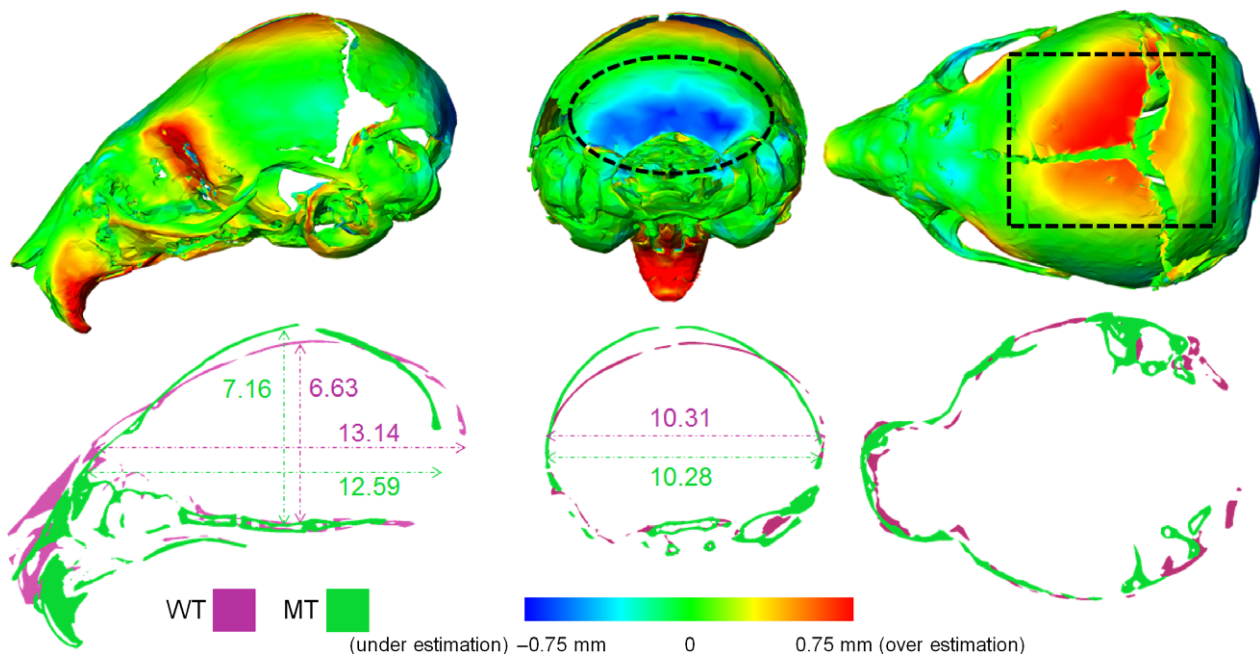
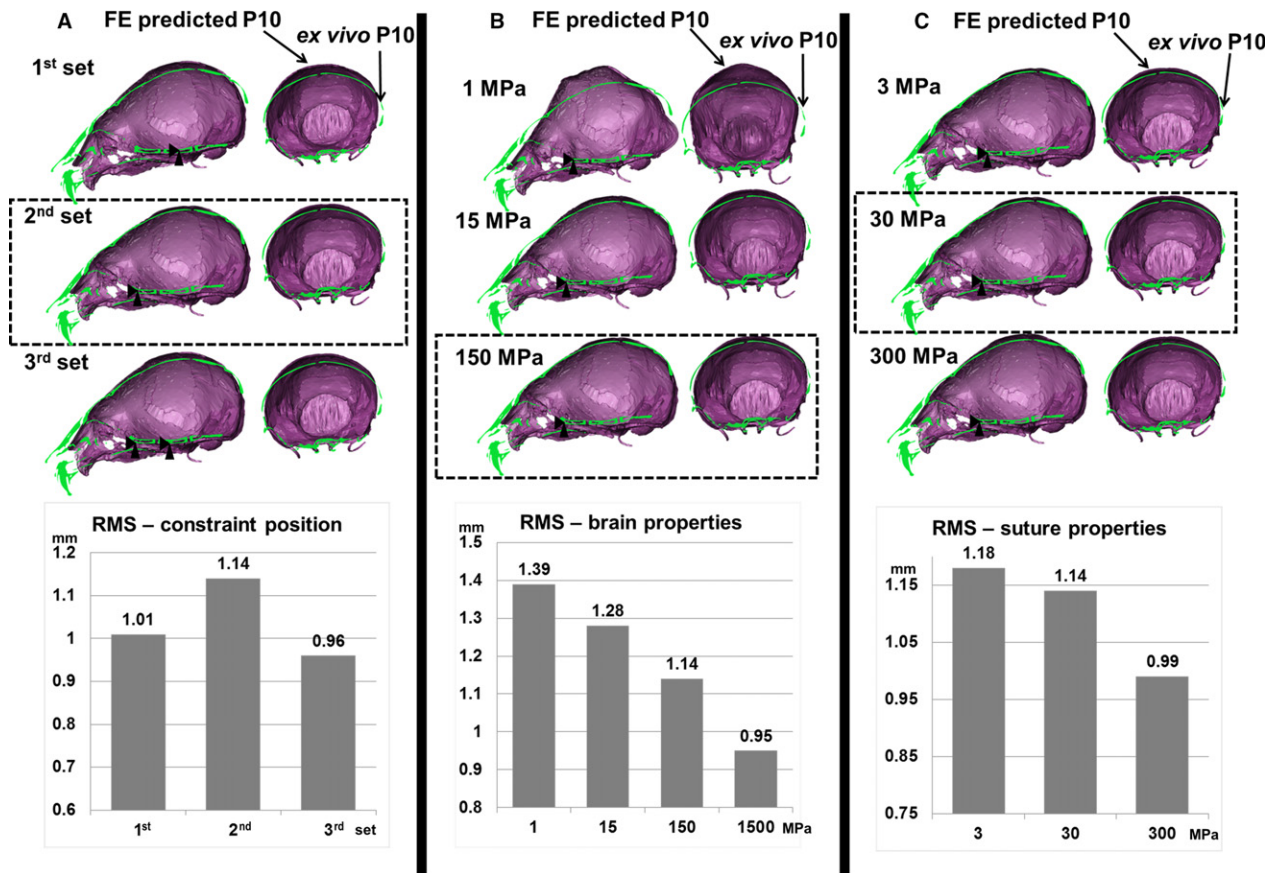


Fig. 6 3D morphological comparison between the *ex vivo* P10 wild-type (WT) and mutant type (MT) mice. The highlighted oval shows the overall shorter length of the MT skull in comparison with the WT skull; the square shows its extended height.



**Fig. 7** Sensitivity analysis to the choice of (A) boundary condition, (B) elastic modulus of the brain and (C) sutures. Dashed outlines highlight the baseline values and results. The sagittal section of the average *ex vivo* P10 is shown in green; the purple figures show the finite element (FE) predictions.

the *ex vivo* P10 skull based on the baseline model parameters. The FE model overestimates the skull height by 0.56 mm (highlighted square in Fig. 8, 7.19 vs. 6.63 mm) and underestimates the skull length by 0.21 mm (highlighted oval in Fig. 8, 12.93 vs. 13.14 mm). In contrast, using the same parameters, the FE model simulating the MT mice skull shape also overestimates the skull height by 0.16 mm (Fig. 9, 7.32 vs. 7.16 mm) and underestimates the skull length by 0.13 mm (Fig. 9, 12.72 vs. 12.59 mm).

## Discussion

Calvarial growth is thought to involve a series of complex biological, chemical and perhaps mechanical signals between a number of soft and hard tissues such as the growing brain, dura mater, sutures and bone (Morriss-Kay & Wilkie, 2005; Richtsmeier & Flaherty, 2013; Al-Rekabi et al. 2016). This study aimed to investigate whether a simple biomechanical approach simulating expansion of the brain can predict calvarial growth in WT and a mouse model of craniosynostosis. The study focused on prediction of calvarial growth up to P10, using FE methodology, which corresponds to about 1 year of age in humans, the point at

which there is clinical consensus advocating surgical treatment of craniosynostosis. To validate the FE results, a series of morphological studies on WT and MT mice were carried out.

The morphological studies highlighted: (i) expansion of the calvaria up to P20 in both WT and MT; (ii) centric growth of the cranial base; (iii) that the MT mice have a shorter skull length than WT mice and display bulging across the parietal region, in line with previous studies (Eswarakumar et al. 2004; Peryn et al. 2006; Liu et al. 2013; Martínez-Abadías et al. 2013; Peskett et al. 2017). Most importantly, (iv) they provided the reference data required for validation of the FE modelling approach.

Sensitivity analysis to investigate the choice of input parameters is a key step in any FE study, therefore a series of sensitivity tests were carried out initially to understand their impact on the results. In the studies performed, the FE results consistently overestimated the calvarial height and underestimated the calvarial width (Fig. 7). The results highlighted that the brain (or, here, the intracranial filling material) properties had the highest impact on the predictions. The elastic modulus of the brain is reported to be in the range of 1–30 kPa (Bouchonville et al. 2016). This is three to

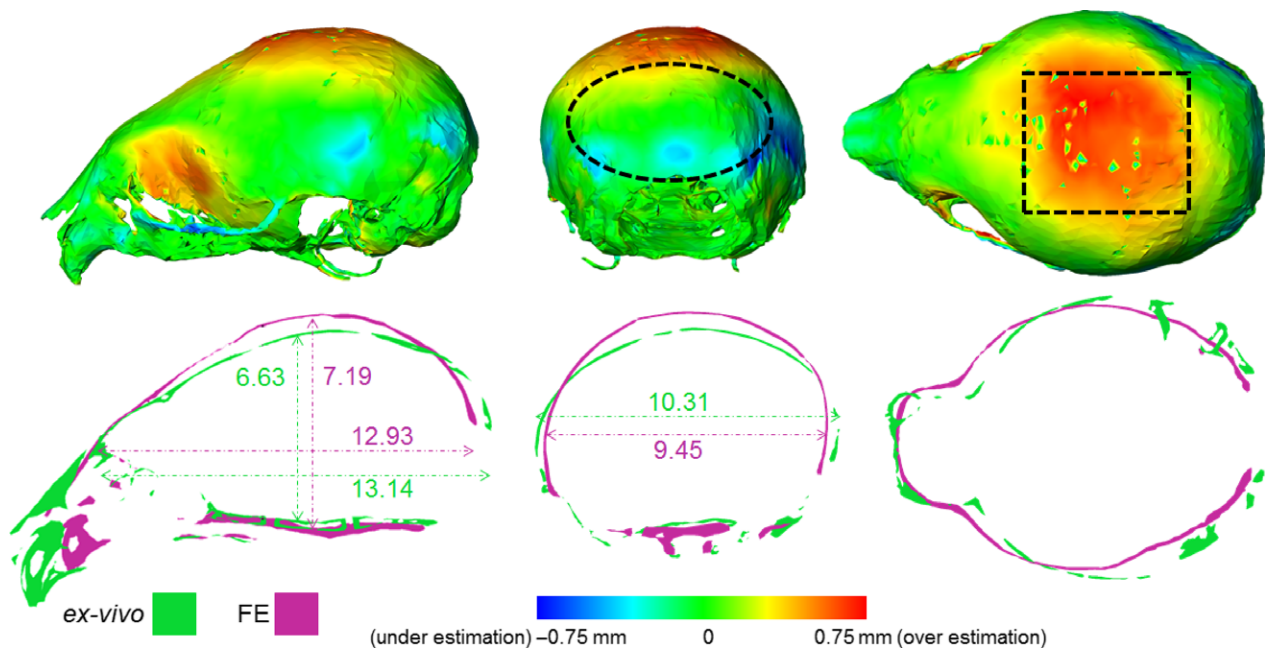


**Fig. 8** 3D morphological comparison between the finite element (FE) predicted and *ex vivo* wild-type mouse at P10. The length is underestimated (the oval), whereas the height is overestimated (the square).

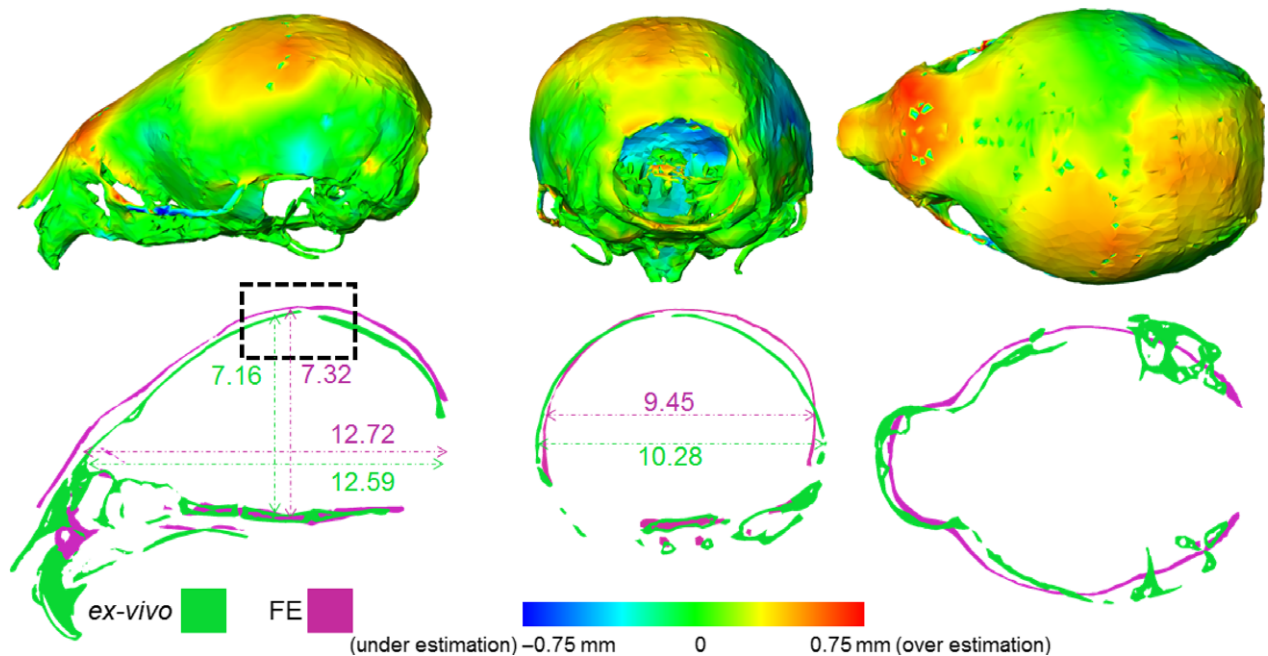


**Fig. 9** 3D morphological comparison between the finite element (FE) predicted and *ex vivo* mutant type mouse at P10. There is a relatively good match between the FE prediction and *ex vivo*.

four orders of magnitude lower than the baseline value of 150 MPa used in this study. This may appear unrealistic, nonetheless, as it generally leads to a similar degree of calvarial expansion to the *ex vivo* data it may have compensated the effect of other tissues not included here. For instance, dura mater was not modelled explicitly in this

study and is expected to have an elastic modulus in the range of 1–1000 MPa (e.g. van Noort et al. 1981; Maikos et al. 2008). Although it is not clear what the combined elastic modulus of the intracranial soft tissues is, it is likely to be higher than each of its individual components and it is perhaps covered in the range of properties tested in the

sensitivity tests here. Although higher values of elastic modulus for brain lead to a better match with the *ex vivo* data, 150 MPa was chosen as the baseline having investigated the sensitivity of the model to this parameter.

Overall, the FE models predicted the expansion of the WT and MT model skulls from P3 to P10 reasonably well. However, there were differences between the FE results and the *ex vivo* measurements at P10 (Figs 8 and 9). The fact that the FE prediction constantly overestimates the skull height might be due to not modelling the soft tissues that cover the brain and perhaps constrain it to the base of the skull, i.e. dura mater. On the other hand, although we believe that at early stages of postnatal development, a uniform growth of the brain is not an unrealistic assumption, it is likely that in mouse from about P10 onward, brain growth deviates from a uniform radial growth in line with the bone formations at the sutures to exhibit a more posterior growth (see also Fig. 5).

To the best of our knowledge this is the first attempt to predict calvarial growth in WT and craniosynostotic MT mice using FE analysis. A similar approach was recently tested in humans to predict normal calvarial growth up to 1 year of age, and it also showed promising results (Libby et al. 2017). Nonetheless, there are a number of limitations to the current approach that can be addressed: (i) several anatomical structures were not explicitly modelled; for example, the dura mater will constrain the brain expansion to some degree; (ii) bone forms gradually at the suture, its thickness and elastic modulus increases during the development, coincident with skull expansion (Richtsmeier & Flaherty, 2013; Moazen et al. 2015, 2016). It is likely that addition of these changes to the model described in this study can enhance the presented prediction and may lead to better matching of the skull height predictions.

Considering the limitations mentioned above, modelling an expanding brain using our methodology, seems to predict skull expansion reasonably well. This suggests that brain growth may be a key factor in the morphogenesis of the calvarial growth. Future studies are required to address the limitations of the approach, nonetheless this approach may have applications in improving management of craniosynostosis, for example through optimization of the reconstruction methods for the different various forms of the condition. In the longer term, this could reduce the number of re-operations for children displaying the condition and enhance their quality of life.

## Acknowledgements

This work was supported by the Royal Academy of Engineering (grant no. 10216/119 to M.M.).

## Conflict of interest

The authors have no conflict of interest to declare.

## Authors' contribution

M.M., C.B. and M.J.F. designed the study, A.M. performed the study, A.M., J.L., M.M. and E.P. performed the analysis, A.M., M.M., M.J.F., C.B. and E.P. wrote the paper. All authors gave final approval for publication.

## References

- Aggarwal M, Zhang J, Miller MI, et al. (2009) Magnetic resonance imaging and micro-computed tomography combined atlas of developing and adult mouse brains for stereotaxic surgery. *Neuroscience* **162**, 1339–1350.
- Al-Rekabi Z, Cunningham ML, Sniadecki NJ (2016) Cell mechanics of craniosynostosis. *ACS Biomater Sci Eng* **3**, 2733–2733. <https://doi.org/10.1021/acsbomaterials.6b00557>.
- Bouchonville N, Meyer M, Gaude C, et al. (2016) AFM mapping of the elastic properties of brain tissue reveals kPa  $\mu\text{m}^{-1}$  gradients of rigidity. *Soft Matter* **12**, 6232–6239.
- Boulet SL, Rasmussen SA, Honein MA (2008) A population-based study of craniosynostosis in metropolitan Atlanta, 1989–2003. *Am J Med Genet A* **146A**, 984–991.
- Chuang N, Mori S, Yamamoto A, et al. (2011) An MRI-based atlas and database of the developing mouse brain. *NeuroImage* **54**, 80–89.
- Claessens M, Sauren F, Wismans J (1997) Modeling of the human head under impact conditions: a parametric study. SAE Technical Paper 973338.
- Cohen MM (2005) Editorial: perspectives on craniosynostosis. *Am J Med Genet A* **136A**, 313–326.
- Cornelissen M, Ottelander Bd, Rizopoulos D, et al. (2016) Increase of prevalence of craniosynostosis. *J Craniomaxillofac Surg* **44**, 1273–1279.
- Cox PG, Rayfield EJ, Fagan MJ, et al. (2012) Functional evolution of the feeding system in rodents. *PLoS ONE* **7**, e36299.
- Curtis N, Jones MEH, Shi J, et al. (2011) Functional relationship between skull form and feeding mechanics in *Sphenodon* and implications for Diapsid skull development. *PLoS ONE* **6**, e29804.
- Dekaban AS (1977) Tables of cranial and orbital measurements, cranial volume, and derived indexes in males and females from 7 days to 20 years of age. *Ann Neurol* **2**, 485–491.
- Eswarakumar VP, Horowitz MC, Locklin R, et al. (2004) A gain-of-function mutation of *Fgfr2c* demonstrates the roles of this receptor variant in osteogenesis. *Proc Natl Acad Sci USA* **101**, 12555–12560.
- Gefen A, Margulies SS (2004) Are in vivo and in situ brain tissues mechanically similar? *J Biomech* **37**, 1339–1352.
- Grova M, Lo DD, Montoro D, et al. (2012) Models of cranial suture biology. *J Craniofac Surg* **23**, 1954–1958.
- Gussekkloo SW, Berthaume MA, Pulaski DR, et al. (2017) Functional and evolutionary consequences of cranial fenestration in birds. *Evolution* **71**, 1327–1338.
- Henderson JH, Chang LY, Song HM, et al. (2005) Age-dependent properties and quasi-static strain in the rat sagittal suture. *J Biomech* **38**, 2294–2301.
- Herring SW (2008) Mechanical influences on suture development and patency. *Front Oral Biol* **12**, 41–56.
- Holmes G (2012) The role of vertebrate models in understanding craniosynostosis. *Childs Nerv Syst* **28**, 1471–1481.
- Johnson D, Wilkie AOM (2011) Craniosynostosis. *Eur J Hum Genet* **19**, 369–376.

- Kupczik K, Dobson CA, Fagan MJ, et al. (2007) Assessing mechanical function of the zygomatic region in macaques: validation and sensitivity testing of finite element models. *J Anat* **210**, 41–53.
- Li Z, Luo X, Zhang J (2013) Development/global validation of a 6-month-old pediatric head finite element model and application in investigation of drop-induced infant head injury. *Comput Methods Programs Biomed* **112**, 309–319.
- Libby J, Marghoub A, Johnson D, et al. (2017) Modelling human skull growth: a validated computational model. *J R Soc Interface* **14**, 20170202.
- Liu J, Nam HK, Wang E, et al. (2013) Further analysis of the Crouzon mouse: effects of the FGFR2(C342Y) mutation are cranial bone-dependent. *Calcif Tissue Int* **92**, 451–466.
- Maikos JT, Elias RA, Shreiber DI (2008) Mechanical properties of dura mater from the rat brain and spinal cord. *J Neurotrauma* **25**, 38–51.
- Martínez-Abadías N, Motch SM, Pankratz TL, et al. (2013) Tissue-specific responses to aberrant FGF signaling in complex head phenotypes. *Dev Dyn* **242**, 80–94.
- van der Meulen J, van der Hulst R, van Adrichem L, et al. (2009) The increase of metopic synostosis a pan-European observation. *J Craniofac Surg* **20**, 283–286.
- Miller K, Chinzei K, Orssengo G, et al. (2000) Mechanical properties of brain tissue in-vivo: experiment and computer simulation. *J Biomech* **33**, 1369–1376.
- Moazen M, Costantini D, Bruner E (2013) A sensitivity analysis to the role of fronto-parietal suture in *Lacerta bilineata*: a preliminary finite element approach. *Anat Rec* **296**, 198–209.
- Moazen M, Peskett E, Babbs C, et al. (2015) Mechanical properties of calvarial bones in a mouse model for craniosynostosis. *PLoS ONE* **10**, e0125757.
- Moazen M, Alazmani A, Rafferty K, et al. (2016) Intracranial pressure changes during mouse development. *J Biomech* **49**, 123–126.
- Mooney MP, Siegel MI, Burrows AM, et al. (1998) A rabbit model of human familial, nonsyndromic, unicoronal suture synostosis: part 1. Synostotic onset, pathology, and sutural growth patterns. *Childs Nerv Syst* **14**, 236–246.
- Morriss-Kay GM, Wilkie AOM (2005) Growth of the normal skull vault and its alteration in craniosynostosis: insights from human genetics and experimental studies. *J Anat* **207**, 637–653.
- van Noort R, Black MM, Martin TR, et al. (1981) A study of the uniaxial mechanical properties of human dura mater preserved in glycerol. *Biomaterials* **2**, 41–45.
- Opperman LA (2000) Cranial sutures as intramembranous bone growth sites. *Dev Dyn* **485**, 472–485.
- Perlyn CA, DeLeon VB, Babbs C, et al. (2006) The craniofacial phenotype of the Crouzon mouse: analysis of a model for syndromic craniosynostosis using three-dimensional MicroCT. *Cleft Palate Craniofac J* **43**, 740–748.
- Peskett E, Kumar S, Baird W, et al. (2017) Analysis of the Fgfr2<sup>C342Y</sup> mouse model shows condensation defects due to misregulation of Sox9 expression in prechondrocytic mesenchyme. *Biol Open* **6**, 223–231.
- Rayfield EJ (2007) Finite element analysis and understanding the biomechanics and evolution of living and fossil organisms. *Annu Rev Earth Planet Sci* **35**, 541–576.
- Richtsmeier JT, Flaherty K (2013) Hand in glove: brain and skull in development and dysmorphogenesis. *Acta Neuropathol* **125**, 469–489.
- Ross CF, Patel BA, Slice DE, et al. (2005) Modeling masticatory muscle force in finite element analysis: sensitivity analysis using principal coordinates analysis. *Anat Rec* **283A**, 288–299.
- Sperber GH (1989) *Craniofacial Embryology* (4th edn). London: Wright, Butterworths. 102 pp.
- Szwedowski TD, Fialkov J, Whyne CM (2011) Sensitivity analysis of a validated subject-specific finite element model of the human craniofacial skeleton. *Proc Inst Mech Eng H* **225**, 58–67.
- Toro-Ibacache V, Fitton LC, Fagan MJ, et al. (2016) Validity and sensitivity of a human cranial finite element model: implications for comparative studies of biting performance. *J Anat* **228**, 70–84.
- Wilkie AOM (1997) Craniosynostosis: genes and mechanisms. *Hum Mol Genet* **6**, 1647–1656.
- Wolanski W, Larysz D, Gzik M, et al. (2013) Modeling and biomechanical analysis of craniosynostosis correction with the use of finite element method. *Int J Numer Method Biomed Eng* **29**, 916–925.